Published in final edited form as:
Cancer Res. 2013 April 1; 73(7): 2235–2246. doi:10.1158/0008-5472.CAN-12-1851.

mTOR inhibitors block Kaposi sarcoma growth by inhibiting essential autocrine growth factors and tumor angiogenesis

Debasmita Roy[1,3], **Sang-Hoon Sin**[2,3], **Amy Lucas**[2,3], **Raman Venkataramanan**[4], **Ling Wang**[2,3], **Anthony Eason**[2,3], **Veenadhari Chavakula**[2,3], **Isaac B. Hilton**[1,3], **Blossom Damania**[1,2,3], and **Dirk P. Dittmer**[1,2,3,*]

[1]Curriculum in Genetics and Molecular Biology, University of North Carolina at Chapel Hill

[2]Department of Microbiology and Immunology, University of North Carolina at Chapel Hill

[3]Lineberger Comprehensive Cancer Center, University of North Carolina at Chapel Hill

[4]Department of Pharmaceutical Sciences, University of Pittsburgh

Abstract

Kaposi's Sarcoma (KS) originates from endothelial cells and it is one of the most overt angiogenic tumors. In Sub-Saharan Africa, where HIV and the Kaposi Sarcoma-associated Herpes Virus (KSHV) are endemic, KS is the most common cancer overall, but model systems for disease study are insufficient. Here we report the development of a novel mouse model of KS where KSHV is retained stably and tumors are elicited rapidly. Tumor growth was sensitive to specific allosteric inhibitors (rapamycin, CCI-779, RAD001) of the pivotal cell growth regulator mTOR. Inhibition of tumor growth was durable up to 130 days and reversible. mTOR blockade reduced VEGF secretion and formation of tumor vasculature. Together, the results demonstrated that mTOR inhibitors exert a direct anti-KS effect by inhibiting angiogenesis and paracrine effectors, suggesting their application as a new treatment modality for KS and other cancers of endothelial origin.

Keywords

Kaposi's Sarcoma (KS); Kaposi's Sarcoma-associated Herpes Virus (KSHV); Human Herpes Virus-8 (HHV8); Rapamycin; mTOR; Angiogenesis; Vascular Endothelial Growth Factor (VEGF); CCI-779; RAD001

INTRODUCTION

Kaposi's Sarcoma (KS) is an aggressive cancer of the endothelial cell origin affecting immune compromised patients, the elderly as well as children and adults in Sub-Saharan Africa. KS is the most common cancer overall (men and women) in Namibia, Botswana, Zimbabwe, Zambia, Malawi, Mozambique, Uganda, Ethiopia and parts of South Africa (1). KS is an AIDS defining malignancy. It is regularly seen as a solid organ transplant associated cancer in Southern Europe, the Mediterranean region, Turkey and Saudi Arabia (2). Chang et al. identified Kaposi's Sarcoma-associated Herpes Virus (KSHV) in any and all forms of KS (3). For lack of known tumor-specific target pathways, KS is treated with cytotoxic chemotherapy, now predominantly liposomal doxorubicin (Doxil™). Although,

*Corresponding Author: University of North Carolina at Chapel Hill, 116 Manning Drive, CB# 7290, Chapel Hill, NC 27599-7290, Phone: (919) 966-7962, Fax: (919) 962-8103, ddittmer@med.unc.edu.

The authors disclose no potential conflicts of interest.

initial response rates are reasonable, subsequent failures are not uncommon (4). Drug resistance has also been documented. Doxil™ is associated with toxicity and has a lifetime dose limit. This motivated our experiments to establish a novel animal model for drug evaluation and to explore the PI3K/Akt/mTOR pathway as a new target of intervention in KS.

Morphologically, KS lesions appear as flat dermal 'patches' upon initial presentation. As the lesion progresses, it goes from patch to plaque to nodule and the initial red color takes on a darker, purplish hue. The characteristic color of these lesions is indicative of the high degree of vasculogenesis and angiogenesis associated with KS. Angiogenesis in KS begins even before the formation of a visible lesion. 100% of the KS tumor cells carry KSHV and express the KSHV latency associated nuclear antigen (LANA) as the defining biomarker for KS (5, 6). The tumor cells also express other viral proteins, which promote tumor cell growth cell-autonomously or through induction of soluble factors, which act through autocrine and paracrine mechanisms.

vGPCR is the KSHV homolog to human IL8 receptor; it can signal in the absence of ligand binding, thus resulting in a constitutively active state (7–9). vGPCR can activate phospho-inositide-3-Kinase (PI3K) as well as induce Vascular Endothelial Growth Factor (VEGF) (10). Other viral signaling molecules, which can activate PI3K signaling, include K1 and K15 (11, 12). As multiple (K1, K15, vGPCR) viral signaling molecules converge on the PI3K pathway, we reasoned that KS is addicted to this pathway and that kinases within this pathway represent promising drug targets.

PI3K is activated by membrane receptor signaling and phosphorylates its downstream target Akt. Phosphorylated Akt in turn activates the mTOR kinases, which have multiple targets that support cell growth (reviewed in (13, 14)). We, along with other groups, have shown that the PI3K/Akt/mTOR pathway is constitutively activated in KS-infected cells as well as in vGPCR and K1 driven cell culture models (12, 15–18).

Clinical observations also supported the importance of the PI3K/Akt/mTOR pathway in KS. Stallone et al. (19) reported that switching the immune suppressive regimen of renal transplant patients from CyclosporinA, which inhibits cyclophillin in T-cells, to rapamycin (sirolimus), which inhibits mTOR (20), resulted in regression of KS lesions. Others have reported similar cases (21–23); a few exceptions have also been noted (24, 25). Most recently we completed a pilot study of AIDS-KS and found long-term disease stabilization or partial responses in 6 of 7 (85%) HIV-positive patients (26). These clinical studies allowed for two alternative hypotheses as to the mechanism of rapamycin and other allosteric mTOR inhibitors (everolimus, temsirolimus), the so-called rapalogs (reviewed in (27)). First, rapalogs changed either the type or the level of immune suppression and KS tumor regression was secondary. This hypothesis is supported by the sometimes spontaneous regression of KS after immune reconstitution of AIDS patients or after immune suppression tampering of transplant recipients. Second, rapalogs have direct anti-tumor effects as had been demonstrated for everolimus in renal cell cancer and temsirolimus in mantle cell lymphoma (28–30). These anti-tumor effects could be impacting the tumor cell directly or the supporting vasculature. Unique to KS both the tumor cell itself and the tumor-feeding blood vessels are of endothelial origin.

To decide among these competing hypotheses we established a novel mouse model of KS, which is dependent on the KSHV virus, and used it to evaluate a battery of structurally different, FDA approved mTOR inhibitors: rapamycin/ Sirolimus, everolimus/ RAD-001 and Temsirolimus/ CCI-779. As controls we used Cyclosporine A and FK506 (Tacrolimus), which is a macrolide that is structurally related to rapamycin, but does not inhibit mTOR

(31). The latter control drugs modulate the immune status as efficiently as rapamycin, but have no activity against mTOR. We found that all three rapalogs were equally effective in multiple KS models. Rapalogs inhibited VEGF-1 secretion and arrested growth in immune deficient mice by reducing intra-tumor ribosomal S6 phosphorylation, tumor growth and neoangiogenesis. In this model rapamycin was superior to doxorubicin.

METHODS

Cell culture

All cell lines were cultured in DMEM supplemented with 100 μg/ml streptomycin sulphate, 100 U/ml penicillin G (Life Technologies, Carlsbad, CA, USA), and 10% FBS at 37°C in 5% CO_2. Cell lines were obtained from the ATCC or derived in our laboratory. The cells have been tested and authenticated. The method used was whole genome Affymetrix 6.0 SNP array. The cells were last tested by the aforementioned method at submission within receipt or resuscitation from stock. The L1T2 cell line will be submitted to the ATCC.

Quantitative PCR for KSHV Genome

Genomic DNA was extracted using Wizard SV Genomic DNA Purification System, as per manufacturer's protocol (Promega, Madison, WI) and quantitative PCR (qPCR) was used to detect the viral genome in the different KS cell lines as per our previous publications (32).

CGH Analysis

Genomic DNA was extracted as above and hybridized to the 6.0 GeneChip Human Mapping Array that uses >906 600known SNP and 946 000 CNV markers (Affymetrix). Data analysis was performed using Partek Genomics Suite as described previously (33), and normalized to tert-immortalized human vein endothelial cell (HUVEC).

Immunofluorescence

Cells were cultured overnight on glass coverslips in 6-well plates (Falcon-BD Biosci. Inc, San Jose, CA). They were then washed in PBS followed by protocol for immune fluorescence as described(34). Primary mouse anti-LANA (1:600 dil.) (Novocastra Lab Ltd., Newcastle, UK), rabbit anti-S6 ribosomal protein, Alexa Fluo® 488 conjugated anti-phospho-S6 ribosomal protein for both S235/236 and S240/244 residues (1:200 dil.) (Cell Signaling Tech., Inc., MA) were used for immunofluorescence. Images were taken on LEICA DM4000B fluorescence microscope (Leica, Heidelberg, Germany) equipped with a 63/1.4–0.6 numerical aperture (NA) objective and a Q-Imaging Retiga 2000RV camera. Raw microscopy image stacks were deconvoluted using Simple PCI™ (Hamamatsu Corp., Sewickley, PA, USA) 2D Blind Deconvolution that iteratively applies AutoQuant Imaging (Media Cybernetics, Inc. Bethesda, MD) proprietary algorithm to remove blur and generate high clarity images, and stored as tiff files. Images were assembled in Photoshop CS4 under MacOsX 10.7.

Tumor formation

Cells were counted, washed once in ice-cold phosphate-buffered saline (PBS, Cellgro Mediatech, Inc., Herndon, VA) and indicated cell doses were diluted into 100 μl PBS and mixed with 100 μl growth factor-depleted Matrigel (BD Biosciences, Bedford, MA). $1x10^6$ cells were injected sub-cutaneously into the flank of C.B.17-$Pkrdc^{SCID}$ mice (Jackson Laboratory, Bar Harbor, MN) following our previously validated procedures (35). The mice were observed every day for the presence of palpable tumors. Drug or vehicle was injected intra-peritoneally at the indicated dosing schedule. Tumor diameters were determined by caliper measurements. Tumor volume calculated as V = a * b * c, where a, b and c are the

three diameters (length, breadth and width) of the tumor. The tumors were excised from the site of injection and fixed in formalin (Fisher Diagnostics, Middletown, VA) for subsequent analysis.

Blood Rapamycin Quantification

Blood was collected from the animals by cardiac puncture 48hrs after the last intra-peritoneal injection of Rapamycin at either 2.5 mg/kg or 5 mg/kg dose. Care was taken to ensure that blood was directly collected into EDTA-coated tubes (BD, Franklin Lakes, NJ) to prevent any coagulation. Rapamycin levels were determined from whole blood by HPLC-MS-MS using Nova_Pak® columns (Waters Corp, Milford, MA) offering sensitivity in the 2–50 ng/ml range.

Immunohistochemistry

Tumors were removed and processed as per (17) and stained using the appropriate primary antibodies: phospho-S6 ribosomal protein (Ser 235/236) monoclonal antibody (1:100 dil.) and phospho-4EBP1 (Ser 65) antibody (1:50 dil.) from Cell Signaling Inc. (Boston, MA). Sections were imaged using a LEICA DM LA histology microscope (Leica, Heidelberg, Germany) equipped with a 10x/0.25 numerical aperture (NA), a 40x/0.75 NA N plan objective, or HC PLAN APO 20x/0.70 NA and Leica DPC 480 camera. Images were stored as TIFF files under Mac OS X10.5. Staining intensity was assessed using the FRIDA (Framework for Image Dataset Analysis) as outlined (36). Briefly, FRIDA measures the pixel intensity of the tumor section based on a user defined ‘positive’ stain and we plotted the square root of this total area intensity. To determine the degree of significance, we used ANOVA implemented in the R statistics environment (version 2.14.1).

Tumor Vasculature Staining

Tumor vasculature was determined using commercially available Periodic Acid Schiff (PAS) staining system following manufacturer’s recommendations (Sigma Aldrich, St. Louis, MO). Sections were imaged, PAS staining quantified using FRIDA and significance determined, as above.

VEGF Quantification

VEGF levels in the culture supernatants were determined using commercially available VEGF ELISA assay as per manufacturer’s recommendations (PeproTech, Rocky Hill, NJ). The biological activity of secreted VEGF (supplemental figure 1) was ascertained by sprouting assay as described (37).

RESULTS

A robust, human, KSHV-positive mouse model for KS

Despite the identification of KS nearly two decades ago, there is a dearth of pre-clinical models for KS. Explants from KS biopsies have been successful to a limited degree (two cell lines in 20 years (38, 39)) but rapidly lose the viral episome. Thus they no longer represent the full spectrum of molecular interactions present in the primary tumor. The best-characterized example until recently was the SLK cell line. It was isolated from an oral KS biopsy of an HIV-negative male (38) and at the time of tissue procurement expressed KSHV LANA and exhibited the KS defining spindle cell morphology. KSHV was lost, but the spindle cell morphology was retained and SLK cells form tumors in immune deficient mice. This year it was shown that the SLK cell line used in laboratories throughout the world has in fact become contaminated with the kidney carcinoma cell line Caki-1; a second KS-

derived cell line KS-Y1 was also shown to be contaminated by an irrelevant cell line (40). This leaves the field bereft of human tumor models for this cancer.

De novo infection of human endothelial cells in culture by KSHV is possible, but here too the virus is rapidly lost unless maintained under drug selection (37, 41–43). The exceptions are two cell lines (TIVE-E1 and TIVE-L1) that were derived by infection of telomerase-immortalized, umbilical cord-derived endothelial cells (44). These cells maintain KSHV in the absence of drug selection, secrete IL6, IL8, VEGF and form tumors in nude mice, albeit slowly.

The L1T2 cell line was established from a sub-cutaneous tumor that developed upon injecting TIVE-L1 cells into C.B.17-Pkrdc^{SCID} mice (figure 1, panel A). L1T2 retained the tumor forming potential of the parental cell line. They induced uniform, fast growing, sub-cutaneous (s.c.) tumors in C.B.17-Pkrdc^{SCID} (figure 1, panel B) and nu/nu mice (data not shown). At the 10^6 cells dose 100% of the animals developed palpable tumors after only 2 days, which grew exponentially for up to 21 days (Table 1). This phenotype held true at the 10^5-cells dose as well (data not shown). The cells express the viral latent protein LANA in the typical punctate pattern (Figure 1, panel C). The punctate pattern requires the presence of KSHV terminal repeats which bind LANA (45), and the so-called “LANA-dots” correlate directly with the number of viral episomes (46). The L1T2 induced tumors were highly proliferative as demonstrated by Ki-67 staining (Figure 2, panel A–B), and in the tumor retained expression of the endothelial marker genes CD31 (Figure 2, panel E–F) and VEGF-R3 (Figure 2, panel C–D) as well as LANA (Figure 2, panel G–H). The cells retained the complete viral episome as demonstrated by real-time qPCR with primers in each orf across the genome (Figure 2, panel J). L1T2, for the first time, provides an animal model for KS based on human cells, that maintains the virus in the absence of selection, that is fast, economic, robust and reproducible enough for large scale *in vivo* drug evaluation.

Rapamycin is efficacious against KS xenograft tumors *in vivo*

To test the hypothesis that rapalogs have direct anti-tumor activity against KS and that this activity is independent of any immune modulating properties that these agents may also have, we treated established xenografts in C.B.17-Pkrdc^{SCID} mice that lack any immune effector cells with rapamycin and its various analogs. First, we tested TIVE-E1 and TIVE-L1 cells, which had previously been established as model systems to study KS pathogenesis in nu/nu mice (44). TIVE E1 and L1 represent two independent clones of telomerase-immortalized, KSHV infected endothelial cells, each of which sustained independent chromosome rearrangements (Figure 2, panel J). TIVE-L1 (figure 3, panel A) and TIVE-E1 (figure 3, panel B) cells were injected s.c. and upon formation of palpable tumors, animals received rapamycin at 3 mg/kg/day 3 times a week, or vehicle. Figure 3 panels A and B compare tumor growth in rapamycin and mock treated animals. In each cohort drug treated animals showed significantly smaller tumors than mock treatment ($p<0.05$ by repeated measurements, random effects model). Next, we tested KSHV-negative SLK cells, which thus far were the standard for pre-clinical drug testing in KS (figure 3, panel C). Upon formation of palpable tumors, animals received rapamycin at 2.5 mg/kg/day 3 times a week, 5 mg/kg/day 3 times a week, or vehicle. At 5 mg/kg Rapamycin was very effective against tumor progression; however, it adversely affected overall health of the animals (table 1). At 2.5mg/kg of Rapamycin was equally as effective in tumor inhibition as 5 mg/kg/day dose together with improvement in survival and overall health ($p<0.05$ by repeated measurements random effects model). Finally, we tested KSHV-positive L1T2 cells (figure 3, panel D). Upon formation of palpable tumors, animals received rapamycin at 2.5mg/kg/day 3 times a week, or vehicle. Again, rapamycin effectively inhibited tumor growth compared to vehicle control ($p<0.05$ by repeated measurements random effects model).

To establish equivalency amongst the different rapalogs we also tested temsirolimus and everolimus in the L1T2 system. Each resulted in significant tumor inhibition. We also tested the ATP-competitive mTOR inhibitor PP242 (table 1). This resulted in tumor reduction, but was not superior to allosteric rapalogs. FK506, which is structurally similar to rapamycin, and which like rapamycin binds FKBP (but not mTOR), had no activity (table 1). Table 1 is a summary of all the studies we conducted. These show that rapalogs are efficacious against tumors, irrespective of whether they were isolated from KS biopsies (SLK) or generated following de novo infection of endothelial cells (E1, L1, L1T2). Single agent rapalogs, irrespective of their particular structure, resulted in prolonged (up to 130 days) growth inhibition. Of note, each experiment was conducted in parallel with a similar size group of mock treated animals, which received the same cell aliquot. The group size n in table 1 refers only to the size of the experimental group. In total we observed significant raplog-dependent tumor inhibition in 85 animals.

Rapalog dosing presents a significant challenge in the clinic, especially considering that rapalogs are metabolized by the cytochrome P450 family members in the liver (47). Even in culture, the IC50 for rapamycin may vary more than 1000-fold between cancer cell lines (48). The reason is unknown and may have as much to do with drug transport as with pathway resistance mutations. P450 is expressed by the tumor endothelial cells within KS lesions (Roy and Dittmer, unpublished). Therefore, we optimized the dosing regimen required to obtain therapeutic drug trough levels, while minimizing toxicity. Note that our dosing is rather infrequent compared to other experimental designs (16, 49), which require daily dosing. At 5mg/kg doses of rapamycin the animals exhibited weight loss, lethargy and had to be sacrificed despite robust inhibition of tumor progression. At 1.5mg/kg, the animals remained healthy throughout extended treatment, but anti-tumor activity was lost (data not shown). Based on these data we established the optimal dose for long-term rapamycin treatment in C.B.17.PKRD^{scid} mice at 2.5 mg/kg 3 times a week. Next, we assessed the actual levels of Rapamycin in the blood stream of the animals. Figure 2, panel F shows that at 2.5mg/kg doses we are able to maintain a steady level of drug in the blood compared to 5mg/kg (figure 2, panel E) where blood levels spike early on and presumably cause drug toxicity. In summary, we established the efficacy of multiple, chemically distinct rapalogs (sirolimus/rapamycin, temsirolimus, everolimus), and the ATP-competitive mTOR inhibitor PP242 in four distinct xenograft models of KS. We established 2.5 mg/kg 3 times a week as a low intensity regimen, which resulted in long-term (> 60 days) growth suppression and showed that this dosing regimen leads to sustained, systemic trough levels of 20 ng/ml, which was the target trough levels in recent clinical trials of this drug family (26).

Rapamycin inhibits phosphorylation of mTOR targets S6-ribosomal protein and 4E-Binding Protein in vivo

Having extensively validated our tumor model, we used it to elucidate the mechanism of action of allosteric rapalogs in KS. Phosphorylation of ribosomal S6 (S6R) protein is considered a robust readout for mTOR activation. We treated L1T2 cells with rapamycin (5 μM corresponding to 4.5μg/ml) in culture and measured S6 phosphorylation. Figure 4 shows immunofluorescence staining for total (panels A and D) and phosphorylated S6R (pS6R) (panels B, E for pS6R (Ser235/236) and panels C, F for pS6R (Ser240/244)). As expected S6 is expressed at high levels in L1T2 cells and heavily phosphorylated at both composite sites (figure 4, panels A, B and C). Upon treatment with rapamycin, total S6 expression remained unchanged, while S6 phosphorylation was completely abolished (without loss of cell viability). This demonstrates that rapalogs inhibit their molecular targets in our KS-tumor model.

Because we were treating established tumors in the mouse model where rapalogs lead to sustained growth inhibition, and only later leads to necrosis due to lack of nutrient and

oxygen (see below), we were able to measure molecular markers of mTOR inhibition in early tumors *in vivo*. The L1T2 tumor morphology of mock treated tumors was analogous to KS biopsies as judged by Hematoxilin stain. The drug treated tumors were similar, except that the interior of the tumor mainly consisted of necrotic tissue, compared to mock (data not shown). Treatment with rapamycin resulted in dramatically reduced levels of pS6R (Ser235/236) compared to both mock and FK506 treatment (figure 4, panels G–I). In addition to pS6R, a second target of mTOR is 4EBP1 (14, 50). Immunohistochemical staining of tumor sections revealed down-regulation of 4EBP1 phosphorylated at Ser65 following rapamycin treatment, but no change in mock and FK506 treated tumors (figure 4, panels J–L). Rapamycin reduced S6 and 4E-BP1 phosphorylation *in vivo* (figure 4, panel M, with $p \leq 0.05$ by two-way ANOVA). This demonstrates that the molecular mechanism of action of rapalogs in KS is the same as in other cancers, such as KSHV-associated primary effusion lymphoma (PEL) (17). It validates the use of pS6 and p4E-BP1 as novel biomarkers for rapalog therapy in KS.

Rapamycin inhibits VEGF secretion and associated vasculature development

KS tumors are characterized by their atypical purple color indicative of vastly increased vasculature and angiogenesis. Furthermore, KS tumors are rich in VEGF, IL-1beta, PDGF and other endothelial cell growth factors (51–53). This phenotype is recapitulated in our murine model. Rapalogs are known to inhibit endothelial-cell mediated tumor neo-angiogenesis in addition to direct tumor growth (54, 55). We therefore hypothesized that some of the KS-specific targets of rapamycin are paracrine growth factors involved in tumor vasculature development. Because of the endothelial cell lineage of KS tumors, these same growth factors can also function in an autocrine manner, which may explain the increased sensitivity of KS to rapalogs.

VEGF is a key angiogenesis-promoting factor secreted by KS and other tumor cells. TIVE-E1, -L1, SLK and L1T2 cells all secrete VEGF, as detected in the culture supernatant. We measured between 2,000 – 4,000 pg/ml in the supernatant KS-like cells over a 48-hour period. By comparison, KSHV-infected lymphoma cell lines secreted 200 – 400 pg/ml in the same, luminex-based, assay. The cells secreted similarly high levels of IL-6 and IL-8 (Roy and Dittmer, unpublished). Rapamycin down regulated levels of VEGF secreted by TIVE-L1 cells in culture (figure 5, panel A). We conducted a time course followed by drug washout experiment to assess both the production and accumulation of VEGF in culture supernatant. We detected levels of secreted VEGF (isoform A) in cells treated with 0.5μM (0.45μg/ml) and 5μM (4.5ug/ml) rapamycin over 96-hours (figure 5, panel A). Upon drug withdrawal, the cells recovered slowly and gradually increased VEGF secretion. Similar results were noted for TIVE-L1, SLK and L1T2 cells (data not shown). For KSHV infected BCBL-1 cells, we found that conditioned media from rapamycin treated cells no longer supported HUVEC tubule formation (supplemental figure 1). This demonstrates that rapamycin inhibits biologically active VEGF, which is an autocrine growth factor in KS (56).

The xenograft model constitutes a much more demanding setting than *in vitro* culture and requires cancer cells to establish and maintain an optimal microenvironment for survival. We hypothesized that reduction of growth factors by rapalogs would have a pronounced impact on tumor progression. To address this, we utilized PAS staining, which marks the vasculature directly, rather than relying on just one particular biomarker protein, thereby detecting the overall physiological impact (57, 58). Rapamycin resulted in a sustained tumor vasculature defect (figure 5, panels B). Rapamycin-treated tumors had less ordered, less mature vessel formation compared to mock and FK506 treatment. The tumor cells appeared in isolated, clumped nests rather than each cell being enmeshed in supportive stroma and vasculature with the KS associated slit-like morphology. Quantification of PAS-positivity

demonstrated a statistically significant reduction in staining (figure 5, panel C). Rapamycin-treated tumors had significantly reduced branching indicative of immature vasculature and poor angiogenesis. Since clinically KS is among the most highly angiogenic sarcomas, second only to hemangioma, we conclude that reduction of growth of tumor supporting endothelial cells by rapalogs and inhibition of paracrine factors (like VEGF) contributes to the efficacy of the rapalogs against this particular cancer.

Rapamycin and Doxorubicin combination therapy

Having demonstrated single-agent efficacy of multiple rapalogs against KS, we explored the efficacy of rapamycin in the adjuvant setting. Specifically, we wanted to test the hypothesis that adding doxorubicin to rapamycin would result in increased cytotoxicity. We confirmed this hypothesis in the cell culture model of PEL (supplemental Figure 2); however the *in vivo* studies yielded a surprising result. Pre-formed L1T2 tumors were treated with four different regimens: (1) 2.5mg/kg Rapamycin (intra-peritoneally (i.p.) 3x weekly), (2) 4 mg/kg Doxorubicin (i.p. 5x weekly), (3) 2.5mg/kg Rapamycin (i.p. 3x weekly) + 4 mg/kg Doxorubicin (i.p. 5x weekly) or (4) mock. Individually, both drugs inhibited tumor progression (table 1). Nonetheless, the combination treatment did not show synergy or an additive effect on tumor growth. We utilized PAS staining to investigate tumor angiogenesis (figure 6). As expected untreated L1T2 tumors were highly vascularized and individual cells were neatly packed in a supportive, mesh-like vascular microenvironment (figure 6, panel B and C). Rapamycin treatment (panels D, E) destroyed the tumor vasculature ($p \leq 0.005$ by Wilcox Sum Rank test), which we quantified by counting the number of PAS positive branches in several tumor sections. Branch points, defined as two or more finger-like PAS vessels at a common point, were averaged from five distinct regions for each tumor section. Doxorubicin did not affect the tumor vasculature (figure 6, panel A). The combination treatment shows a novel phenotype: tumor cells were nested together in relatively few islands separated by extended thicker slit-like structures (figure 6, see panel H and I and double arrows). This may explain the absence of synergy between rapamycin and doxorubicin in this model. By restricting angiogenesis rapamycin restricts at the same time the flow of nutrients and oxygen to the tumor (resulting in growth inhibition) and the flow of the doxorubicin drug, thus limiting the efficacy of the cytotoxic drug. This result has important clinical ramifications. It argues against simultaneous therapy of rapalogs and cytotoxic drugs, which in the extreme may foster the emergence of drug resistant tumor cells due to sub-optimal exposure to the cytotoxic drug.

DISCUSSION

A large body of clinical evidence suggests that in the solid organ transplant setting switching to a rapamycin containing immune suppressive regimen leads to KS regression or lowers the risk of KS development (21–23, 59, 60). Similar data are missing for AIDS KS, endemic KS or classic KS or for the use of rapalogs as dedicated, single agent anti-tumor drugs against KS. No data exist for the newer rapamycin analogs everolimus, temsirolimus, or the ATP-competitive inhibitors of mTOR (27). Here, we tested the hypothesis that mTOR inhibitors have anti-tumor activity against KS, and we describe a new mechanism that could explain the extraordinary sensitivity of KS to rapamycin. This work was predicated on development of a new human tumor model of KS, which is robust, fast and mimics all the phenotypes associated with the human tumor (figure 1). It was driven by the insights that (i) KS is an endothelial cell lineage tumor (42, 61, 62), (ii) KS is dependent on autocrine and paracrine growth factors, (iii) extensive neoangiogenesis and, (iv) rapalogs stymy tumor growth in common cancers by inhibiting the host endothelial cells comprising the tumor vasculature and microenvironment as well as through direct inhibition of tumor cell activity (14).

For the purpose of this discussion we define rapalogs functionally as inhibitors of mTOR, as opposed to FK506, which has a similar chemical structure as rapamycin, but does bind to or inhibit mTOR. All rapalogs tested induced tumor regression of preformed KS-like human tumors in our xenograft model (figure 2, table 1). Rapalog efficacy did not depend on immune system modulation, since the host animals were deficient for B, T and NK cells and since we achieved long-term, sustained responses with a 3x per week dosing regimen. Rapalog efficacy did not depend on the presence of KSHV, since KSHV-negative SLK cell tumors were also inhibited. This is expected since SLK cells exhibit the same signs of PI3K/Akt/mTOR activation, i.e. phosphorylation of key residues, as KS tumors (36), and as KSHV-induced KS cell lines. Rapalogs decreased phosphorylation of S6 ribosomal protein and 4EBP-1 *in vivo* (figure 4), demonstrating that they inhibit the intended molecular targets downstream of mTOR. The anti-tumor effect was reversible *in vivo*: upon withdrawal of the rapalogs the tumors grew back uniformly (supplemental figure 3). In contrast, two chemically related drugs Cyclosporine-A (data not shown) and FK506 had no anti-tumor effect. This is particularly interesting since FK506 like rapamycin also binds to FKBP12, but cannot bind mTOR (63). It supports the specificity of action of the rapalogs. The ATP-competitive inhibitor PP242 also inhibited tumor progression *in vivo*, but was not superior to the allosteric mTOR inhibitors. This validates mTOR as a bona-fide drug target in KS and provides a solid biological rationale for future clinical trials.

We uncovered a novel mechanism of action for mTOR inhibitors that is specific to KS. The rapalogs inhibited VEGF secretion by the KS tumor cells (figure 3) as well as VEGF secretion in KSHV-dependent lymphomas (supplemental figure 2). We surmise that the translational arrest induced by mTOR inhibition is not universal, but preferentially affects autocrine growth factors of endothelial lineage cells and KS tumor cells. This is analogous to the situation in PEL, where we showed previously that rapamycin stopped lymphoma growth by inhibiting the essential autocrine growth factors IL6 and IL10 (17). This may explain the differential response of different human cancers to rapalogs. Cancers, like KS, that still depend heavily on pro-angiogenic and growth factors to sustain elevated PI3K signaling are susceptible to mTOR inhibitors. Cancers that evolved growth factor independence such as hormone resistant prostate cancer or estrogen receptor negative breast cancer may be less responsive to mTOR inhibitors.

Finally, we explored the combination therapy of rapamycin with the prototypic cytostatic drug, doxorubicin, which represents the current standard of care for KS. We did not find any benefit of combining these two drugs *in vivo*. This represents a cautionary note in regards to combining mTOR inhibitors with other drugs, as mTOR inhibitors may inhibit neovascularization and sprouting of non-transformed endothelial cells (figure 6), thereby potentially limiting drug delivery to the tumor.

Supplementary Material

Refer to Web version on PubMed Central for supplementary material.

Acknowledgments

This work was supported by NIH grant CA163217 to DPD and BD. The UNC animal models core facility was supported in part by NIH grant P30CA06086 to the Lineberger Comprehensive Cancer Center.

References

1. Jemal A, Bray F, Forman D, O'Brien M, Ferlay J, Center M, et al. Cancer burden in Africa and opportunities for prevention. Cancer. 2012

2. Ganem D. KSHV and the pathogenesis of Kaposi sarcoma: listening to human biology and medicine. The Journal of clinical investigation. 2010; 120:939–49. [PubMed: 20364091]
3. Chang Y, Cesarman E, Pessin MS, Lee F, Culpepper J, Knowles DM, et al. Identification of herpesvirus-like DNA sequences in AIDS-associated Kaposi's sarcoma. Science. 1994; 266:1865–9. [PubMed: 7997879]
4. Cianfrocca M, Lee S, Von Roenn J, Tulpule A, Dezube BJ, Aboulafia DM, et al. Randomized trial of paclitaxel versus pegylated liposomal doxorubicin for advanced human immunodeficiency virus-associated Kaposi sarcoma: evidence of symptom palliation from chemotherapy. Cancer. 2010; 116:3969–77. [PubMed: 20564162]
5. Dupin N, Fisher C, Kellam P, Ariad S, Tulliez M, Franck N, et al. Distribution of human herpesvirus-8 latently infected cells in Kaposi's sarcoma, multicentric Castleman's disease, and primary effusion lymphoma. Proceedings of the National Academy of Sciences of the United States of America. 1999; 96:4546–51. [PubMed: 10200299]
6. Dittmer D, Lagunoff M, Renne R, Staskus K, Haase A, Ganem D. A cluster of latently expressed genes in Kaposi's sarcoma-associated herpesvirus. J Virol. 1998; 72:8309–15. [PubMed: 9733875]
7. Molden J, Chang Y, You Y, Moore PS, Goldsmith MA. A Kaposi's sarcoma-associated herpesvirus-encoded cytokine homolog (vIL- 6) activates signaling through the shared gp130 receptor subunit. J Biol Chem. 1997; 272:19625–31. [PubMed: 9235971]
8. Wan X, Wang H, Nicholas J. Human herpesvirus 8 interleukin-6 (vIL-6) signals through gp130 but has structural and receptor-binding properties distinct from those of human IL-6. J Virol. 1999; 73:8268–78. [PubMed: 10482577]
9. Arvanitakis L, Geras-Raaka E, Varma A, Gershengorn MC, Cesarman E. Human herpesvirus KSHV encodes a constitutively active G-protein-coupled receptor linked to cell proliferation. Nature. 1997; 385:347–50. [PubMed: 9002520]
10. Sodhi A, Montaner S, Patel V, Zohar M, Bais C, Mesri EA, et al. The Kaposi's sarcoma-associated herpes virus G protein-coupled receptor up-regulates vascular endothelial growth factor expression and secretion through mitogen-activated protein kinase and p38 pathways acting on hypoxia-inducible factor 1alpha. Cancer Res. 2000; 60:4873–80. [PubMed: 10987301]
11. Brinkmann MM, Schulz TF. Regulation of intracellular signalling by the terminal membrane proteins of members of the Gammaherpesvirinae. The Journal of general virology. 2006; 87:1047–74. [PubMed: 16603506]
12. Wang L, Dittmer DP, Tomlinson CC, Fakhari FD, Damania B. Immortalization of primary endothelial cells by the K1 protein of Kaposi's sarcoma-associated herpesvirus. Cancer Res. 2006; 66:3658–66. [PubMed: 16585191]
13. Vivanco I, Sawyers CL. The phosphatidylinositol 3-Kinase AKT pathway in human cancer. Nat Rev Cancer. 2002; 2:489–501. [PubMed: 12094235]
14. Sabatini DM. mTOR and cancer: insights into a complex relationship. Nat Rev Cancer. 2006; 6:729–34. [PubMed: 16915295]
15. Uddin S, Hussain AR, Al-Hussein KA, Manogaran PS, Wickrema A, Gutierrez MI, et al. Inhibition of phosphatidylinositol 3′-kinase/AKT signaling promotes apoptosis of primary effusion lymphoma cells. Clin Cancer Res. 2005; 11:3102–8. [PubMed: 15837766]
16. Bhatt AP, Bhende PM, Sin SH, Roy D, Dittmer DP, Damania B. Dual inhibition of PI3K and mTOR inhibits autocrine and paracrine proliferative loops in PI3K/Akt/mTOR-addicted lymphomas. Blood. 2010; 115:4455–63. [PubMed: 20299510]
17. Sin SH, Roy D, Wang L, Staudt MR, Fakhari FD, Patel DD, et al. Rapamycin is efficacious against primary effusion lymphoma (PEL) cell lines in vivo by inhibiting autocrine signaling. Blood. 2007; 109:2165–73. [PubMed: 17082322]
18. Montaner S, Sodhi A, Pece S, Mesri EA, Gutkind JS. The Kaposi's sarcoma-associated herpesvirus G protein-coupled receptor promotes endothelial cell survival through the activation of Akt/protein kinase B. Cancer Res. 2001; 61:2641–8. [PubMed: 11289142]
19. Stallone G, Schena A, Infante B, Di Paolo S, Loverre A, Maggio G, et al. Sirolimus for Kaposi's sarcoma in renal-transplant recipients. N Engl J Med. 2005; 352:1317–23. [PubMed: 15800227]

20. Baker H, Sidorowicz A, Sehgal SN, Vezina C. Rapamycin (AY-22,989), a new antifungal antibiotic. III. In vitro and in vivo evaluation. J Antibiot (Tokyo). 1978; 31:539–45. [PubMed: 28309]
21. Guenova E, Metzler G, Hoetzenecker W, Berneburg M, Rocken M. Classic Mediterranean Kaposi's sarcoma regression with sirolimus treatment. Archives of dermatology. 2008; 144:692–3. [PubMed: 18490609]
22. Yaich S, Zagdane S, Charfeddine K, Hssairi D, Hachicha J. Simultaneous Hodgkin's disease and Kaposi sarcoma in a renal transplant recipient. Saudi journal of kidney diseases and transplantation : an official publication of the Saudi Center for Organ Transplantation, Saudi Arabia. 2010; 21:306–9.
23. Ho CM, Huang SF, Hu RH, Ho MC, Wu YM, Lee PH. Sirolimus-induced signaling modifications in Kaposi's sarcoma with resolution in a liver transplant recipient. Clinical transplantation. 2010; 24:127–32. [PubMed: 19919613]
24. Boratynska M, Zmonarski SC, Klinger M. Reccurence of Kaposi's sarcoma after increased exposure to sirolimus. International immunopharmacology. 2006; 6:2018–22. [PubMed: 17161356]
25. Babel N, Eibl N, Ulrich C, Bold G, Sefrin A, Hammer MH, et al. Development of Kaposi's sarcoma under sirolimus-based immunosuppression and successful treatment with imiquimod. Transplant infectious disease : an official journal of the Transplantation Society. 2008; 10:59–62. [PubMed: 17428275]
26. Krown SE, Roy D, Lee JY, Dezube BJ, Reid EG, Venkataramanan R, et al. Rapamycin With Antiretroviral Therapy in AIDS-Associated Kaposi Sarcoma: An AIDS Malignancy Consortium Study. J Acquir Immune Defic Syndr. 2012; 59:447–54. [PubMed: 22067664]
27. Dittmer DP, Bhatt AP, Damania B. Rapalogs in viral cancers. Expert opinion on investigational drugs. 2012; 21:135–8. [PubMed: 22214523]
28. Dabora SL, Franz DN, Ashwal S, Sagalowsky A, DiMario FJ Jr, Miles D, et al. Multicenter phase 2 trial of sirolimus for tuberous sclerosis: kidney angiomyolipomas and other tumors regress and VEGF- D levels decrease. PloS one. 2011; 6:e23379. [PubMed: 21915260]
29. Motzer RJ, Escudier B, Oudard S, Hutson TE, Porta C, Bracarda S, et al. Efficacy of everolimus in advanced renal cell carcinoma: a double-blind, randomised, placebo-controlled phase III trial. Lancet. 2008; 372:449–56. [PubMed: 18653228]
30. Hess G, Herbrecht R, Romaguera J, Verhoef G, Crump M, Gisselbrecht C, et al. Phase III study to evaluate temsirolimus compared with investigator's choice therapy for the treatment of relapsed or refractory mantle cell lymphoma. J Clin Oncol. 2009; 27:3822–9. [PubMed: 19581539]
31. Kino T, Hatanaka H, Miyata S, Inamura N, Nishiyama M, Yajima T, et al. FK-506, a novel immunosuppressant isolated from a Streptomyces. II. Immunosuppressive effect of FK-506 in vitro. J Antibiot (Tokyo). 1987; 40:1256–65. [PubMed: 2445722]
32. Fakhari FD, Jeong JH, Kanan Y, Dittmer DP. The latency-associated nuclear antigen of Kaposi sarcoma-associated herpesvirus induces B cell hyperplasia and lymphoma. The Journal of clinical investigation. 2006; 116:735–42. [PubMed: 16498502]
33. Roy D, Sin SH, Damania B, Dittmer DP. Tumor suppressor genes FHIT and WWOX are deleted in primary effusion lymphoma (PEL) cell lines. Blood. 2011; 118:e32–9. [PubMed: 21685375]
34. Chen W, Hilton IB, Staudt MR, Burd CE, Dittmer DP. Distinct p53, p53:LANA, and LANA complexes in Kaposi's Sarcoma--associated Herpesvirus Lymphomas. J Virol. 2010; 84:3898–908. [PubMed: 20130056]
35. Staudt MR, Kanan Y, Jeong JH, Papin JF, Hines-Boykin R, Dittmer DP. The tumor microenvironment controls primary effusion lymphoma growth in vivo. Cancer Res. 2004; 64:4790–9. [PubMed: 15256448]
36. Roy D, Dittmer DP. Phosphatase and tensin homolog on chromosome 10 is phosphorylated in primary effusion lymphoma and Kaposi's sarcoma. The American journal of pathology. 2011; 179:2108–19. [PubMed: 21819957]
37. Wang L, Damania B. Kaposi's sarcoma-associated herpesvirus confers a survival advantage to endothelial cells. Cancer Res. 2008; 68:4640–8. [PubMed: 18559509]

38. Herndier BG, Werner A, Arnstein P, Abbey NW, Demartis F, Cohen RL, et al. Characterization of a human Kaposi's sarcoma cell line that induces angiogenic tumors in animals. AIDS. 1994; 8:575–81. [PubMed: 7520247]
39. Albini A, Paglieri I, Orengo G, Carlone S, Aluigi MG, DeMarchi R, et al. The beta-core fragment of human chorionic gonadotrophin inhibits growth of Kaposi's sarcoma-derived cells and a new immortalized Kaposi's sarcoma cell line. AIDS. 1997; 11:713–21. [PubMed: 9143602]
40. Sturzl M, Gaus D, Dirks WG, Ganem D, Jochmann R. The Kaposi's sarcoma-derived cell line SLK is not of endothelial origin, but is a contaminant from a known renal carcinoma cell line. Int J Cancer. 2012
41. Flore O, Rafii S, Ely S, O'Leary JJ, Hyjek EM, Cesarman E. Transformation of primary human endothelial cells by Kaposi's sarcoma- associated herpesvirus. Nature. 1998; 394:588–92. [PubMed: 9707121]
42. Lagunoff M, Bechtel J, Venetsanakos E, Roy AM, Abbey N, Herndier B, et al. De novo infection and serial transmission of Kaposi's sarcoma-associated herpesvirus in cultured endothelial cells. J Virol. 2002; 76:2440–8. [PubMed: 11836422]
43. Grundhoff A, Ganem D. Inefficient establishment of KSHV latency suggests an additional role for continued lytic replication in Kaposi sarcoma pathogenesis. The Journal of clinical investigation. 2004; 113:124–36. [PubMed: 14702116]
44. An FQ, Folarin HM, Compitello N, Roth J, Gerson SL, McCrae KR, et al. Long-Term-Infected Telomerase-Immortalized Endothelial Cells: a Model for Kaposi's Sarcoma-Associated Herpesvirus Latency In Vitro and In Vivo. J Virol. 2006; 80:4833–46. [PubMed: 16641275]
45. Kedes DH, Lagunoff M, Renne R, Ganem D. Identification of the gene encoding the major latency-associated nuclear antigen of the Kaposi's sarcoma-associated herpesvirus. The Journal of clinical investigation. 1997; 100:2606–10. [PubMed: 9366576]
46. Adang LA, Parsons CH, Kedes DH. Asynchronous progression through the lytic cascade and variations in intracellular viral loads revealed by high-throughput single-cell analysis of Kaposi's sarcoma-associated herpesvirus infection. J Virol. 2006; 80:10073–82. [PubMed: 17005685]
47. Zimmerman JJ. Exposure-response relationships and drug interactions of sirolimus. The AAPS journal. 2004; 6:e28. [PubMed: 15760093]
48. Foster DA, Toschi A. Targeting mTOR with rapamycin: one dose does not fit all. Cell Cycle. 2009; 8:1026–9. [PubMed: 19270529]
49. Sarek G, Kurki S, Enback J, Iotzova G, Haas J, Laakkonen P, et al. Reactivation of the p53 pathway as a treatment modality for KSHV-induced lymphomas. The Journal of clinical investigation. 2007; 117:1019–28. [PubMed: 17364023]
50. Hara K, Yonezawa K, Kozlowski MT, Sugimoto T, Andrabi K, Weng QP, et al. Regulation of eIF-4E BP1 phosphorylation by mTOR. J Biol Chem. 1997; 272:26457–63. [PubMed: 9334222]
51. Samaniego F, Markham PD, Gendelman R, Watanabe Y, Kao V, Kowalski K, et al. Vascular endothelial growth factor and basic fibroblast growth factor present in Kaposi's sarcoma (KS) are induced by inflammatory cytokines and synergize to promote vascular permeability and KS lesion development. The American journal of pathology. 1998; 152:1433–43. [PubMed: 9626048]
52. Sturzl M, Brandstetter H, Zietz C, Eisenburg B, Raivich G, Gearing DP, et al. Identification of interleukin-1 and platelet-derived growth factor-B as major mitogens for the spindle cells of Kaposi's sarcoma: a combined in vitro and in vivo analysis. Oncogene. 1995; 10:2007–16. [PubMed: 7761101]
53. Cornali E, Zietz C, Benelli R, Weninger W, Masiello L, Breier G, et al. Vascular endothelial growth factor regulates angiogenesis and vascular permeability in Kaposi's sarcoma. The American journal of pathology. 1996; 149:1851–69. [PubMed: 8952523]
54. Guba M, von Breitenbuch P, Steinbauer M, Koehl G, Flegel S, Hornung M, et al. Rapamycin inhibits primary and metastatic tumor growth by antiangiogenesis: involvement of vascular endothelial growth factor. Nat Med. 2002; 8:128–35. [PubMed: 11821896]
55. Del Bufalo D, Ciuffreda L, Trisciuoglio D, Desideri M, Cognetti F, Zupi G, et al. Antiangiogenic potential of the Mammalian target of rapamycin inhibitor temsirolimus. Cancer Res. 2006; 66:5549–54. [PubMed: 16740688]

56. Masood R, Cai J, Zheng T, Smith DL, Naidu Y, Gill PS. Vascular endothelial growth factor/vascular permeability factor is an autocrine growth factor for AIDS-Kaposi sarcoma. Proceedings of the National Academy of Sciences of the United States of America. 1997; 94:979–84. [PubMed: 9023368]
57. Folberg R, Hendrix MJ, Maniotis AJ. Vasculogenic mimicry and tumor angiogenesis. The American journal of pathology. 2000; 156:361–81. [PubMed: 10666364]
58. Ocque R, Tochigi N, Ohori NP, Dacic S. Usefulness of immunohistochemical and histochemical studies in the classification of lung adenocarcinoma and squamous cell carcinoma in cytologic specimens. American journal of clinical pathology. 2011; 136:81–7. [PubMed: 21685035]
59. D'Amico F, Fuxman C, Nachman F, Bitetti L, Fauda M, Echevarria C, et al. Visceral Kaposi's sarcoma remission after intestinal transplant. First case report and systematic literature review. Transplantation. 2010; 90:547–54. [PubMed: 20625354]
60. Gutierrez-Dalmau A, Sanchez-Fructuoso A, Sanz-Guajardo A, Mazuecos A, Franco A, Rial MC, et al. Efficacy of conversion to sirolimus in posttransplantation Kaposi's sarcoma. Transplantation proceedings. 2005; 37:3836–8. [PubMed: 16386556]
61. Hong YK, Foreman K, Shin JW, Hirakawa S, Curry CL, Sage DR, et al. Lymphatic reprogramming of blood vascular endothelium by Kaposi sarcoma-associated herpesvirus. Nature genetics. 2004; 36:683–5. [PubMed: 15220917]
62. Boshoff C, Schulz TF, Kennedy MM, Graham AK, Fisher C, Thomas A, et al. Kaposi's sarcoma-associated herpesvirus infects endothelial and spindle cells. Nat Med. 1995; 1:1274–8. [PubMed: 7489408]
63. Brunn GJ, Fadden P, Haystead TA, Lawrence JC Jr. The mammalian target of rapamycin phosphorylates sites having a (Ser/Thr)-Pro motif and is activated by antibodies to a region near its COOH terminus. J Biol Chem. 1997; 272:32547–50. [PubMed: 9405468]

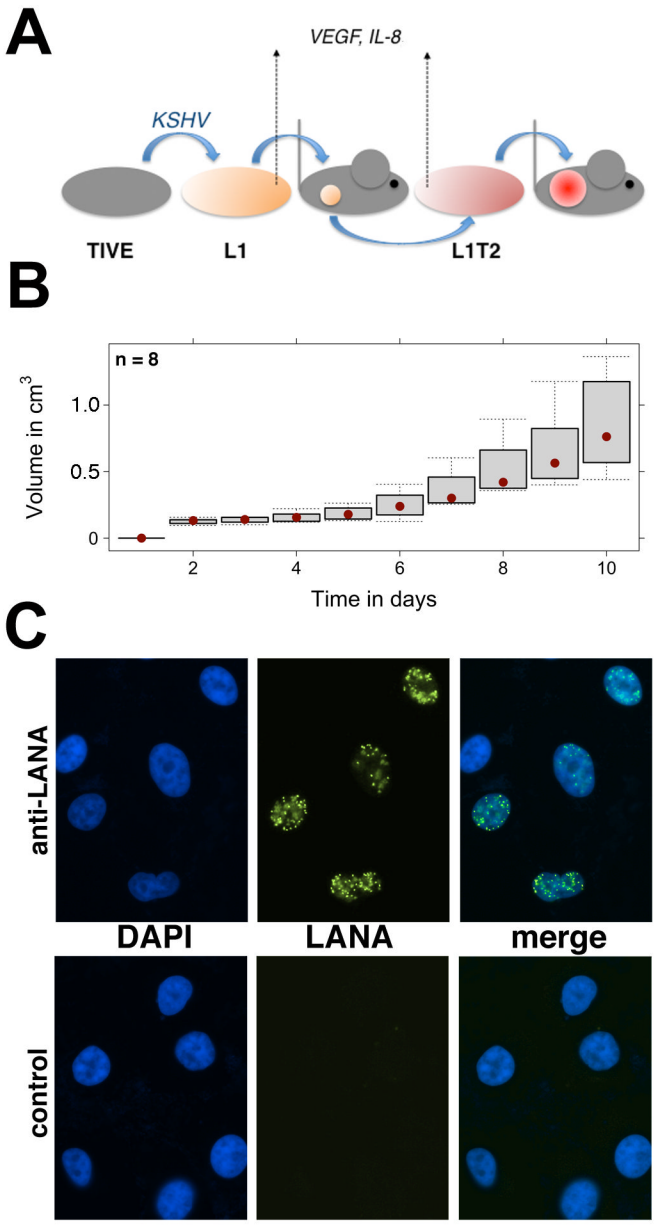

Figure 1. Establishment of L1T2 as a robust KS-like cell line in culture and *in vivo*

Panel A represents the schematic used to isolate L1T2 cells from explanted TIVE-L1 tumors. Cells were explanted from subcutaneous tumors formed in C.B.17-Pkrdc^{SCID} mice injected with TIVE-L1 cells. Both TIVE-L1 and subsequent L1T2 cells secreted pro-angiogenic factors VEGF and IL-8 in culture. Panel B shows a box and wisker plot of tumor onset and progression in C.B.17-Pkrdc^{SCID} mice. The X-axis represents days post-injection and the tumor volume (n = 8) in mm3 on the Y-axis. The red dot denotes the median, the box denotes 25th and 75th percentile, and the whiskers denote the range of the data. Panel C shows immunofluorescence staining for the presence of LANA (green) to indicate the presence of the viral episome in culture. The upper panel is in the presence of anti-LANA primary antibody whereas the lower panel shows secondary only control. The nucleus is counter-stained with DAPI (blue).

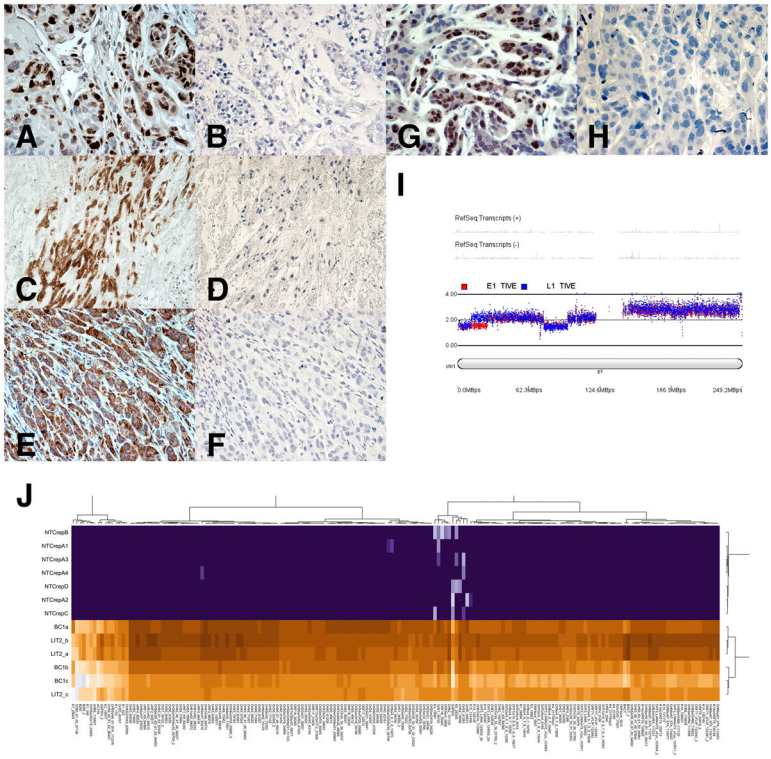

Figure 2. Characterization of the L1T2 cell line

Panel A–H show immunohistochemistry analysis of L1T2 xenografts using antibodies associated with cell proliferation: Ki-67 in panel A, VEGFR-3 in panel C, CD31 in panel E and LANA in panel G. Panels B, D, F and H show the respective no primary antibody control sections on the same slide. Brown indicates the positivity of staining. Nuclei were counterstained with hematoxilin (blue). All images are shown at 200x magnification. Panel I shows the genomic copy number variation across chromosome 1 for the TIVE-E1 (red dots) and TIVE-L1 (blue dots) cell line relative to KSHV-infected, tert-immortalized HUVEC cells analyzed in parallel. Known transcript clusters are indicated on top and chromosome coordinates on bottom, with the heatmap and dot-plot representations of copy number variations in between. The vertical axis refers to the DNA content relative to control. Panel H shows a heatmap representation of real-time qPCR array analysis of total DNA from three independent aliquots (a,b,c) of L1T2 cells using 175 primer pairs distributed across the entire KSHV genome. Aliquots of BC1 cells are used as positive control and water as non-template control (ntc). Red indicates presence and blue represents absence of a discernable PCR product.

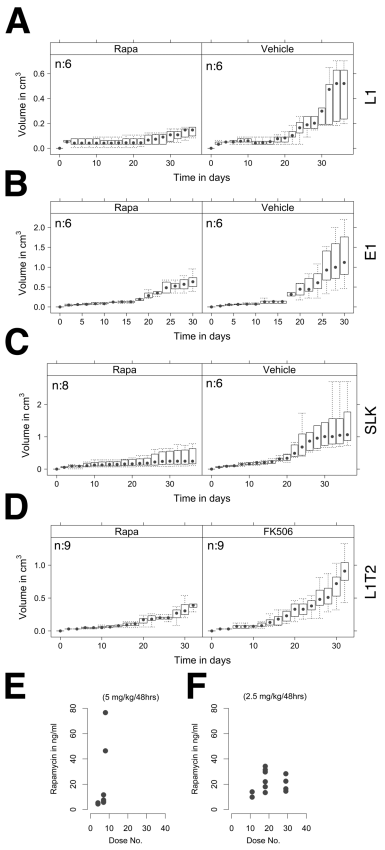

Figure 3. Effect and dosing scheme for rapamycin on different KS-like cell lines

Panels A shows the effect of rapamycin (3mg/kg/day dose) (n = 6) compared to vehicle treatment (n = 6) in TIVE-L1 and panel B in TIVE-E1 xenografts. Panels C shows the effect of rapamycin (2.5mg/kg/day dose) on SLK xenograft tumors (n = 8) compared to vehicle treatment (n = 6). Panel D compares the effectof rapamycin (n = 9) to FK506 (n = 9) treatment against L1T2 xenografts. In each of the panels A–D, the X-axis represents days post-injection and Y-axis shows tumor volume in cm^3. The dot denotes the median, the box denotes 25^{th} and 75^{th} percentile, the whiskers the range of the data. Panel E is the quantification of blood levels of rapamycin 48hrs following the last dose either at 5mg/kg and panel F at 2.5mg/kg dosing concentration. The X-axis represents the total number of doses, either at 2.5mg/kg/day or 5mg/kg/day whereas the actual level of rapamycin in the blood is shown on the Y-axis in ng/ml.

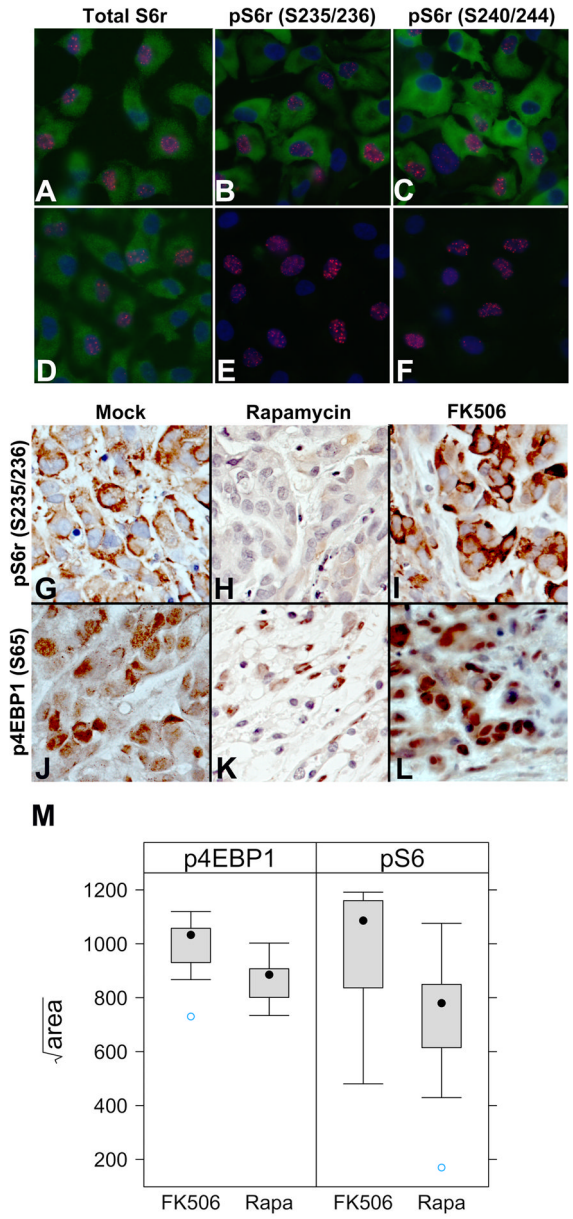

Figure 4. Downregulation of phosphorylated ribosomal S6 protein and eIF4E binding protein (4EBP1) following rapamycin treatment

Panels A–F represent immunofluorescence staining of L1T2 cells. Panels A, B and C represent mock treatment, panels D, E and F are treated with 5uM rapamycin (4.5 μg/ml). Panels A and D represent staining for total S6R protein whereas panels B, E and C, F show S6R phosphorylation on residues S235-236 and S240-244, respectively. This staining is shown in green, the nucleus is in blue (counterstained with DAPI) and KSHV LANA staining in red. Panels G–L show immunohistochemical staining for mTOR downstream effectors pS6R (G, H, I) and p4EBP1 (J, K, L) in tumor sections treated with mock (G, J), 2.5mg/kg rapamycin (H, K) or 2.5mg/kg FK506 (I, L). The nuclei are denoted in blue (Hematoxylin counter-stain). Panel M is the quantification of staining for panels G–L, where the X-axis represents the square root of total area positive for pS6R (S235-236) and p4EBP1 (S65) while the Y-axis are the different treatment groups. The dot denotes the median, the box denotes 25th and 75th percentile, the whiskers the range of the data.

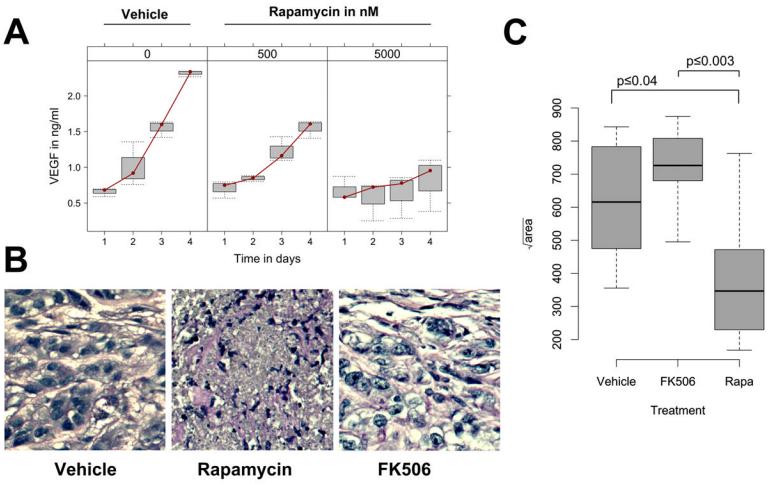

Figure 5. Treatment with rapamycin inhibits angiogenesis

Panel A shows the effect of treatment of TIVE-L1 cells in culture with rapamycin (0.5μM or 5μM) compared to vehicle on secreted levels of VEGF. The X-axis denotes time points in days (up to 96 hours post-treatment) whereas the Y-axis represents mean levels of VEGF in ng/ml. The dot denotes the median, the box denotes 25th and 75th percentile, and the whiskers show the range of the data. Panel B shows representative sections demonstrating the tumor vasculature using PAS staining for vehicle, 2.5mg/kg rapamycin and 2.5mg/kg FK506 treated tumors. PAS marks the mature vasculature in pink to show that treatment with Rapamycin resulted in a near complete disintegration of vascular network within the tumor compared to mock or FK506 treatment. Panel C is the quantification of PAS staining where the X-axis denotes the different treatment groups and the Y-axis represents square root of area of the section that was PAS positive. The line denotes the median, the box denotes 25th and 75th percentile, the whiskers the range of the data. Significance (p-value) is calculated using ANOVA.

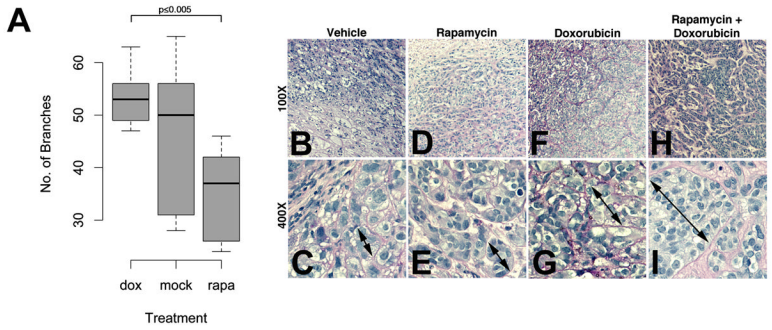

Figure 6. Combination treatment using Rapamycin and Doxorubicin

Panel A shows the number of vascular branches after treatment with vehicle, doxorubicin or rapamycin. The line denotes the median, the box denotes 25th and 75th percentile, and the whiskers the range of the data. Significance (p-value) is calculated using ANOVA. Panel B–I show PAS staining of the tumor for the different treatment groups at 100X and 400X magnifications. Blue/gray indicated cell nuclei and red/purple the surrounding microvasculature. The double arrows provide for a visual aid to gauge the size of the vessel free tumor cell nests.

Table 1

In vivo efficacy studies

Drug	Cell	Drug Conc. (mg/kg)	Progression free (days)	n	Reduction (%)	p ≤
FK506	E1	2.5	41	6	38%	.
	L1T2	2.5	59 #	5	3%	.
	SLK	2.5	46	6	19%	.
Sirolimus/rapamycin	E1	3	37	6	0%	.
		5	41	6	20%	0.05
	L1	3	37	6	166%	0.01
	L1T2	1.25	23	10	83%	.
		1.25	58 #	7	259%	10^{-5}
		2.5	106 #	5	34%	0.04
		2.5	130 #	9	252%	10^{-15}
		2.5	58 #	7	181%	0.0002
		2.5	43	6	203%	0.0007
	SLK	2.5	46	8	282%	0.0001
		2.5	53 #	5	836%	0.0001
		5 *	53 #	5	150%	. *
Doxorubicin	L1T2	4	43	6	51%	0.0004
Sirolimus & Doxorubicin		2.5 +dox	43	7	109%	0.0002
PP242	L1T2	50	27	7	80%	.
Sirolimus & PP242		50 + 2.5	27	7	55%	.
Sirolimus & Ritonavir	L1T2	1.25 +ritonavir	58 #	7	437%	0.0006
		1.25 +ritonavir	23	10	141%	0.05
Temsirolimus/CCl-779	SLK ^	10	78 #	6	307%	10^{-8}
	SLK	10	78 #	6	56%	0.009
Everolimus/RAD001	L1T2	2.5	99 #	7	288%	10^{-6}

Treatment started after palpable tumors (2 mm^2) developed in >= 50% of animals. Each treatment group was compared to a control, vehicle group of similar number of animals that was inoculated simultaneously with the same number of tumor cells. Vehicle-treated animals (control group) require euthanasia between day 20 – 40.

- **i.** "Reduction in volume" shows the % reduction in mean tumor volume in the drug-treated group compared to the vehicle treated group at time point of maximum difference. Typically this was the day when >50% of tumors in the control group grew to 2000 mm^2 and/or required euthanasia.
- **ii.** "progression free" shows the number of days that the animals in the drug-treatment arm remain on study without exponential tumor growth requiring euthanasia or until the experiment was terminated because reduction in tumor volume between matched control and treatment group was significant to p<=0.05.
- **iii.** "n" is the number of animals per drug-treated group. In each experiment these are paired with 5–6 vehicle treated animals that received tumor cells on the same day and from the same passage to allow for direct comparison and calculation of relative reduction in volume.
- **iv.** "conc" lists the concentration of drug. All animals are treated on a Mo, Wed, Fr schedule i.p.
- **v.** p-value as determined using T test of tumor volume at each time point (3 times per week). No value reflects no significant difference to control.

* toxicity in the treatment arm.

progression free survival > 50 days (200% of the untreated group)

^ cells were injected without matrigel support